[Cover Article] Structural and mutational analysis of a monomeric and dimeric form of a single domain antibody with implications for protein misfolding

ARTICLE *in* PROTEINS STRUCTURE FUNCTION AND BIOINFORMATICS · NOVEMBER 2014

Impact Factor: 2.63 · DOI: 10.1002/prot.24671

5 AUTHORS, INCLUDING:

Jaimee R Compton
United States Naval Research Laboratory
15 PUBLICATIONS **55** CITATIONS

SEE PROFILE

Dagmar Leary
United States Naval Research Laboratory
28 PUBLICATIONS **160** CITATIONS

SEE PROFILE

Patricia Legler
United States Naval Research Laboratory
40 PUBLICATIONS **521** CITATIONS

SEE PROFILE

PROTEINS
STRUCTURE ■ FUNCTION ■ BIOINFORMATICS

Structural and mutational analysis of a monomeric and dimeric form of a single domain antibody with implications for protein misfolding

Jade George,[1] Jaimee R. Compton,[2] Dagmar H. Leary,[3] Mark A. Olson,[4] and Patricia M. Legler[3]*

[1] Bowie State University, Bowie, 14000 Jericho Park Road, Maryland 20715-9465

[2] NOVA Research Inc., 1900 Elkin St. Suite 230, Alexandria, Virginia 22308

[3] Department of Cell Biology and Biochemistry, U.S. Army Medical Research Institute of Infectious Diseases, Frederick, Maryland 21702

[4] Naval Research Laboratories, 4555 Overlook Ave., Washington, D.C. 20375

ABSTRACT

Camelid single domain antibodies (sdAb) are known for their thermal stability and reversible refolding. We have characterized an unusually stable sdAb recognizing *Staphylococcal* enterotoxin B with one of the highest reported melting temperatures ($T_m = 85^\circ C$). Unexpectedly, ~10−20% of the protein formed a dimer in solution. Three other cases where <20% of the sdAb dimerized have been reported; however, this is the first report of both the monomeric and dimeric X-ray crystal structures. Concentration of the monomer did not lead to the formation of new dimer suggesting a stable conformationally distinct species in a fraction of the cytoplasmically expressed protein. Comparison of periplasmic and cytoplasmic expression showed that the dimer was associated with cytoplasmic expression. The disulfide bond was partially reduced in the WT protein purified from the cytoplasm and the protein irreversibly unfolded. Periplasmic expression produced monomeric protein with a fully formed disulfide bond and mostly reversible refolding. Crystallization of a disulfide-bond free variant, C22A/C99V, purified from the periplasm yielded a structure of a monomeric form, while crystallization of C22A/C99V from the cytoplasm produced an asymmetric dimer. In the dimer, a significant conformational asymmetry was found in the loop residues of the edge β-strands (S50-Y60) containing the highly variable complementarity determining region, CDR2. Two dimeric assemblies were predicted from the crystal packing. Mutation of a residue at one of the interfaces, Y98A, disrupted the dimer in solution. The pleomorphic homodimer may yield insight into the stability of misfolded states and the importance of the conserved disulfide bond in preventing their formation.

Proteins 2014; 00:000–000.

Key words: misfolded; metastable states; irreversible unfolding; asymmetric; homodimeric; single domain antibody; amyloid-like; fibril; kinetically stable.

INTRODUCTION

The variable domains of immunoglobulins known as v-set domains (~130 amino acids) consist of a β-sandwich of two antiparallel β-sheets connected by a highly conserved disulfide bond. The v-set domain[1] can be found in almost 1000 protein structures within the PDB and is a commonly employed fold used by the immune system to scaffold variable loops and create diverse protein−protein interactions. Single domain antibodies (sdAb) are the recombinantly expressed variable domains, V_HH, of the heavy chain-only antibodies found in shark and camels.[2] They are ~1/10 the size of an immunoglobulin and can bind trace amounts of antigens with low nanomolar dissociation constants. In many cases they reversibly refold even after several cycles of

Additional Supporting Information may be found in the online version of this article.

Structures have been deposited into the PDB: 4TYU, 4U7S, 4U05, 4W70, 4W81, 4W68.

Grant sponsor: DTRA; Grant number: CBCALL12-LS6-2-0036; Grant sponsor: NRL HBCU/MI summer internship program sponsored by the Office of Naval Research (ONR); Grant number: N0001412RX20102; Grant sponsor: ONR/NRL 6.1 base funding.

*Correspondence to: Patricia M. Legler, Naval Research Laboratories, 4555 Overlook Ave., Washington, D.C. 20375. E-mail: patricia.legler@nrl.navy.mil

Received 14 April 2014; Revised 1 August 2014; Accepted 11 August 2014
Published online 18 August 2014 in Wiley Online Library (wileyonlinelibrary.com). DOI: 10.1002/prot.24671

thermal or chemical denaturation,[3,4] making them useful as reliable affinity reagents with minimal requirements for refrigeration or consistent handling. Unlike human antibodies they can be expressed in *E. coli* with good yields.

Proteins with thermodynamic stability have equilibria which favor the folded state and possess relatively moderate free energy barriers between the native and unfolded states; thus, if unfolding occurs refolding is likely. A protein's propensity to unfold is a property routinely quantified by the melting temperature (T_m). Typical sdAb have T_m ranging from 60 to 70°C. Immunization of a llama with Staphylococcal enterotoxin B (SEB) led to the identification of an unusually stable antibody, sdAb A3, with one of the highest reported T_m, 85°C.[5] High T_m values can reflect thermodynamic stability[6,7] or what some have referred to as kinetic stability[8–10] to describe kinetically controlled unfolding. Proteins with high energetic barriers can be stable at high temperatures, but irreversibly denature. A rate-limiting step slows the conversion of the native state to an irreversibly denatured state.[10–13]

$$\text{Native state} \Longleftrightarrow \text{Non-native ensemble} \rightarrow \text{Irreversibly denatured protein} \quad (1)$$

A high energetic barrier can "protect" the native state in harsh environments (e.g., those of thermophilic organisms), since the likelihood of crossing the energetic barrier between the two states at a given temperature is low. As a result the rate of interchange between the states can be on the order of months to years.[10–16] However, near-native misfolded states and non-native states* can have a higher susceptibility towards irreversible alterations or undesirable protein−protein interactions (aggregation), or both. Some kinetically stable proteins form multimers resistant to SDS[17] and stable folding intermediates detectable by size exclusion chromatography.[19] A strong bias towards β-sheet containing proteins is found among kinetically stable proteins, but the significance is unclear.[17]

During the course of crystallization and biochemical characterization of sdAb A3, the WT protein and a disulfide bond-free variant, C22A/C99V,[20] purified from the cytoplasm produced a heterogeneous mixture of monomer and homodimer in solution; however, the mixture still crystallized readily. In solution, we observed only a fraction of the sdAb A3 protein (∼10−20%) in the form of homodimers. A search of the literature revealed three other single domain antibodies where 10−20% of the protein formed homodimers[21–23] and one case where the protein uniformly formed homodimers in solution.[24] As we and others have shown,[21] the monomeric fraction cannot be driven to form additional dimer in solution. This observation suggested that a fraction of the protein was conformationally distinct. Human V_H and V_L domains are known to misfold *in vivo*.[25–28] Thus, we hypothesized that the dimeric fraction of the heterologously expressed V_HH could have arisen from misfolding in the reducing environment of the cytoplasm, and tested this hypothesis by expressing the WT and C22A/C99V proteins in the cytoplasm and periplasm. The first crystal structures of both the monomeric and dimeric forms are presented herein.

Out of >600 human V_H and non-human V_HH domain structures, only 5 homodimeric sdAb structures have been reported;[21–24,29] sdAb A3 is the sixth case. We discuss the commonalities and differences among the few structures of dimeric sdAb that are available, present our methods for producing each of the two states (monomeric and dimeric), and identify a mutant which disrupts the A3 dimer present in solution after cytoplasmic expression. We also examine the reversibility of thermal denaturation of the disulfide bonded and disulfide-bond free variants.

EXPERIMENTAL METHODS

Construction of expression vectors

Protein sequences and general methods are included in the Supporting Information. Two pET22 vectors for periplasmic expression were made: one without a C-terminal His-tag (A3stop) and a second with a C-terminal His-tag (A3peri). A pET15b vector (A3cyto) was made for cytoplasmic expression of an N-terminal His-tagged protein containing a thrombin cleavage site. Site-directed mutagenesis was done using a QuikChange™ kit (Stratagene).

In silico selection of mutations

Starting conformations for modeling were taken from the crystallographic structure of A3. For modeling mutations at the dimeric interfaces to determine which residues contribute to the stability of the A3 complex, computational alanine scanning was performed using the Robetta server.[30]

Cytoplasmic protein expression and purification

E. coli BL21(DE3) were grown in LB/Ampicllin (50 μg/mL) to an O.D. of ∼1.0. Expression was induced with 0.2 m*M* IPTG, cultures were shaken overnight at 17°C, and cells were pelleted (5,000*g* for 10 min). Protein was purified in the presence or absence of 2 m*M* β-

*Here the non-native ensemble of states in (Eq. (1)) includes partially folded and unfolded states.[11,18] Near-native states which are commonly defined as states retaining >50% of the native contacts and r.m.s.d. < 5 Å arise from the structural plasticity of the native ensemble of states and include intermediate and misfolded states.

mercaptoethanol (BME). The initial crystals were obtained with protein expressed in the cytoplasm and purified in the presence of BME. Cell pellets were lysed in 50 m*M* Tris pH 7.6, 500 m*M* NaCl, 2 m*M* BME, 30 mg lysozyme, and 62.5% BugBuster™ (Novagen), sonicated for 1 min, and then centrifuged for 30 min at 10,000 rpm to pellet the cellular debris. The supernatant was loaded on to a nickel Chelating Sepharose column (30 mL) equilibrated with 50 m*M* Tris pH 7.6, 500 m*M* NaCl, and 2 m*M* BME. The column was washed with the same buffer containing 60 m*M* imidazole and then eluted isocratically with buffer containing 300 m*M* imidazole. The protein was dialyzed against 50 m*M* Tris pH 7.6, 250 m*M* NaCl, 2 m*M* BME with 75 U of thrombin at room temperature (22 ± 3°C). The cut His-tag was removed by running a second nickel column, and thrombin was removed using a 1 mL Benzamidine Sepharose (G.E. Healthcare) column. The protein was diluted 1 : 1 with water and loaded onto an SP-Sepharose column (50 m*M* Tris pH 7.6, 2 m*M* BME). The protein was in the flow through. Size exclusion chromatography was performed using a G-75 Superdex gel filtration column (1 cm x 30 cm, Superdex G75 10/300GL, G.E. Healthcare). The column was equilibrated with either 50 m*M* Tris pH 7.4, 150 m*M* NaCl, or 1x PBS pH 7.4 at 4°C. Column calibration curves were collected for both conditions (Supporting Information) using albumin (66 kDa), carbonic anhydrase (29 kDa), and cytochrome-c (12.4 kDa) from a column calibration kit from Sigma-Aldrich, Inc. For all gel-filtration runs a 0.5 mL loop was filled and used to load the column. The dimer eluted at 11.2 mL and the monomer at 12.8 mL (1x PBS pH 7.4) using a flow rate of 0.5 mL/min.

A calculated extinction coefficient of 23,045 M^{-1} cm^{-1} was used to determine the protein concentration from the A_{280}. Tag-free protein was concentrated to 1.7−33 mg/mL, flash frozen in liquid nitrogen, and stored at −80°C, or stored in 25 m*M* Tris pH 7.6, 125 m*M* NaCl, 50% glycerol at −20°C.

Periplasmic protein purification

Three liter cultures of LB/Amp were inoculated and grown at 37°C to an OD_{600} ~1.0 and induced overnight at 17°C with 0.2 m*M* IPTG. The cells were pelleted and washed with 30 m*M* Tris pH 8.0, 0.5 m*M* EDTA, and 20% sucrose for 10 min at 4°C. The cells were pelleted again at 10,000*g* for 10 minutes and then osmotically shocked (5 m*M* Tris pH 8.0, 1 m*M* EDTA) at 4°C for 1 h with stirring. DNAase was added to avoid sonication. Cells were centrifuged for 30 min at 20,000*g*, and buffer and salt were added (50 m*M* Tris pH 7.6, 150 m*M* NaCl). The protein was loaded onto a nickel column (50 m*M* Tris pH 7.6, 500 m*M* NaCl). The column was washed with 10 column volumes of buffer containing 60 m*M* imidazole and eluted with the same buffer containing 300 m*M* imidazole. The eluate was dialyzed overnight at 4°C (50 m*M* Tris pH 7.6, 150 m*M* NaCl) and for 2 h against 50 m*M* Tris pH 7.6. The protein was loaded onto an SP-Sepharose column (50 m*M* Tris pH 7.6) and eluted in the flow-through. Protein was stored in 25 m*M* Tris pH 7.6, 150 m*M* NaCl, and 50% glycerol at −20°C.

The tag-free A3stop variant was purified by gel-filtration, anion, and cation exchange columns. The osmotic shock was carried out as described above; ammonium sulfate was added to reach 80% saturation. The precipitate was collected by centrifugation and loaded onto a 2.5 × 55 cm G-75 Sephadex gravity column equilibrated with 50 m*M* Tris pH 7.6, 150 m*M* NaCl. Fractions were collected at 4°C, diluted 1 : 5 with 50 m*M* Tris pH 7.6, and loaded onto a Q-Sepharose column equilibrated with 50 m*M* Tris pH 7.6 (Buffer A). Protein was eluted with Buffer B (50 m*M* Tris pH 7.6, 1.0*M* NaCl) using a gradient (100 mL). Protein was concentrated, buffer exchanged, and loaded onto an SP-Sepharose column equilibrated with 50 m*M* Tris pH 7.6 and was found in the flow through.

Crystallization and X-ray diffraction

Initial crystallization conditions were obtained from the Hampton Research (Aliso Viejo, CA) Ammonium Sulfate Grid Screen (HR2–211). The tag-free WT sdAb A3 was buffer exchanged into 50 m*M* Tris pH 7.6 and concentrated to 6.2 mg/mL. Rod-shaped crystals were obtained in hanging drops (1 : 1 protein : precipitant) at 17°C in 0.1*M* citric acid pH 4.1, 1.6*M* ammonium sulfate, 20% glycerol. Crystals were drawn through Paratone-N and flash frozen in liquid nitrogen. The C22A/C99V variant purified from the periplasm (C-terminal His-tag, 2.8 mg/mL) or cytoplasm (tag-removed, 6.0 mg/mL) was crystallized in 0.1*M* HEPES pH 7.0 or 0.1*M* Tris pH 8.0 and 1.6*M* ammonium sulfate and cryoprotected in the same solution containing 30% glycerol. Diffraction data was collected at 150 K using a Bruker Micro-STAR rotating anode equipped with Helios optics and a Bruker Platinum 135 CCD area detector. The structure was solved by molecular replacement using Phaser[31] and a homology model based upon PDB 4DKA.[32,33] Model-building was performed using Coot.[34,35] Simulated annealing was carried out using CNS 1.1,[36] and maximum likelihood refinement with Refmac 5.[37]

Circular dichroism

Thermal denaturation was monitored (2°C per minute) from 20°C to 100°C using a Jasco 810 Circular Dichroism (CD) spectropolarimeter fitted with a Peltier temperature control unit. The melting temperature was determined from a four parameter fit of the ellipticity at

Table I
X-Ray Crystallography Data Collection and Refinement Statistics

	WT (22 days)	WT (5 months)	S74A	C22A/C99Vperi	C22A/C99Vcyto
PDB	4TYU	4U7S	4U05	4W70[e]	4W68
Space group	C222(1)	C222(1)	C222(1)	R3	C222(1)
Unit cell dimensions (Å)	67.20, 72.01, 115.92	67.78, 72.98, 117.16	67.19, 72.17, 117.17	87.83, 87.83, 47.06	66.89,72.04,116.10
Wavelength (Å)	1.54	1.54	1.54	1.54	1.54
Resolution range (Å)[a]	2.12–49.13 (2.12–2.22)	2.07–49.66 (2.16–2.07)	2.50–58.58 (2.50–2.59)	2.28–43.91 (2.28–2.38)	2.00–58.05 (2.11–2.16)
Unique Reflections	15,098	17,180	10,160	6,169	18,197
R_{sym}[b]	0.088	0.066	0.188	0.138	0.104
$I/\sigma I$	12.74 (4.88)	24.28 (5.88)	8.05 (3.95)	9.61(2.79)	16.9 (4.54)
Completeness (%)	92.6 (60.9)	94.9 (79.1)	99.6 (99.6)	100.0(99.9)	100.0 (83.6)
Redundancy	6.45 (2.49)	7.79 (2.45)	7.60 (7.61)	5.30(3.69)	10.57 (3.82)
Refinement statistics					
Resolution (Å)	2.13–45.33	2.07–49.66	2.50–58.59	2.28–43.91	2.00–58.05
No. of reflections	14,320	16,282	9,647	5,880	17,228
R_{factor}[c]	0.239	0.232	0.209	0.190	0.199
R_{free}[d]	0.263	0.242	0.239	0.236	0.242
Number of Atoms					
Protein	1978	1978	1976	986	1978
Solvent	75	115	75	47	103
Other	15	10	15	5	5
Average B–factors (Å^2)					
Protein	9.12 (A), 11.51 (B)	12.71 (A), 14.32 (B)	10.87 (A), 12.16 (B)	15.18	12.98 (A), 15.06 (B)
Solvent	10.46	18.34	10.41	19.88	18.63
Other	18.40	20.58	23.08	38.34	17.53
R.m.s.d. from ideal geometry:					
Bond lengths (Å)	0.006	0.007	0.008	0.008	0.009
Bond angles (degrees)	1.03	1.08	1.12	1.25	1.21
Ramachandran plot					
Most favored regions	92.1%	91.2%	94.7%	91.2%	91.7%
Additional allowed regions	7.9%	8.8%	5.3%	8.8%	8.3%
Generously allowed regions	0.0%	0.0%	0.0%	0.0%	0.0%
Disallowed regions	0.0%	0.0%	0.0%	0.0%	0.0%

[a]Values in parentheses are for the outer most data shell.
[b]R_{sym} was calculated from $R_{sym}=\sum|I_i- < I > |/\sum I_i$
[c]R_{factor} for working set of reflections was calculated using: $R_{factor}=\sum||F_o|-|F_c||/\sum|F_o|$.
[d]R_{free} for test set and size of test set as % total reflections in parentheses.
[e]PDB 4W81 contains the structure at pH 8.0.

205 or 207 nm versus temperature. For T_m measurements the buffer was exchanged to 1x PBS pH 7.4 using PD-10 columns (G.E. Healthcare), and protein was purified with or without gel-filtration using a calibrated G-75 Superdex column. A protein concentration of 7−14 μ*M* and a 1 mm cuvette were used for CD analysis.

RESULTS

Homodimeric structures of the single domain antibody

Several protein expression and purification procedures, as well as constructs (cytoplasmically expressed N-terminal His-tagged, N-terminal tag-removed, periplasmically expressed nonremovable C-terminal His-tagged, and a periplasmically expressed tag-free construct) were prepared (Supporting Information Fig. S1). Two constructs of a disulfide-bond free variant, C22A/C99V, were made that were expressible in the cytoplasm (pet15b plasmid) or periplasm (pet22 plasmid).

The structures were determined by molecular replacement; data collection and refinement statistics are reported in Table I. The WT protein expressed in the cytoplasm readily crystallized at low pH (pH 4.1) (PDB 4TYU, 4U7S). Cytoplasmically and periplasmically expressed C22A/C99V crystallized in conditions differing from WT. C22A/C99V purified from the cytoplasm crystallized as rod-shaped crystals with 2 molecules per asymmetric unit (ASU) at pH 8.0 (PDB 4W68). The monomeric C22A/C99V protein produced in the periplasm crystallized as three-sided pyramids at pH 7.0 (PDB 4W70) and pH 8.0 (PDB 4W81) with 1 molecule per ASU (Fig. 1).

Homodimerization of an sdAb was unexpected as it has only been reported for five other sdAb.[21–24,29] Crystals of the cytoplasmically expressed proteins were grown from protein containing 10−20% homodimer in solution (Fig. 1). The conformation of residues S50-Y60 of CDR2 differed significantly between the two subunits. Residues S50-Y60 formed either a heart-shaped loop (chain A, referred to as the A-form) or a β-hairpin

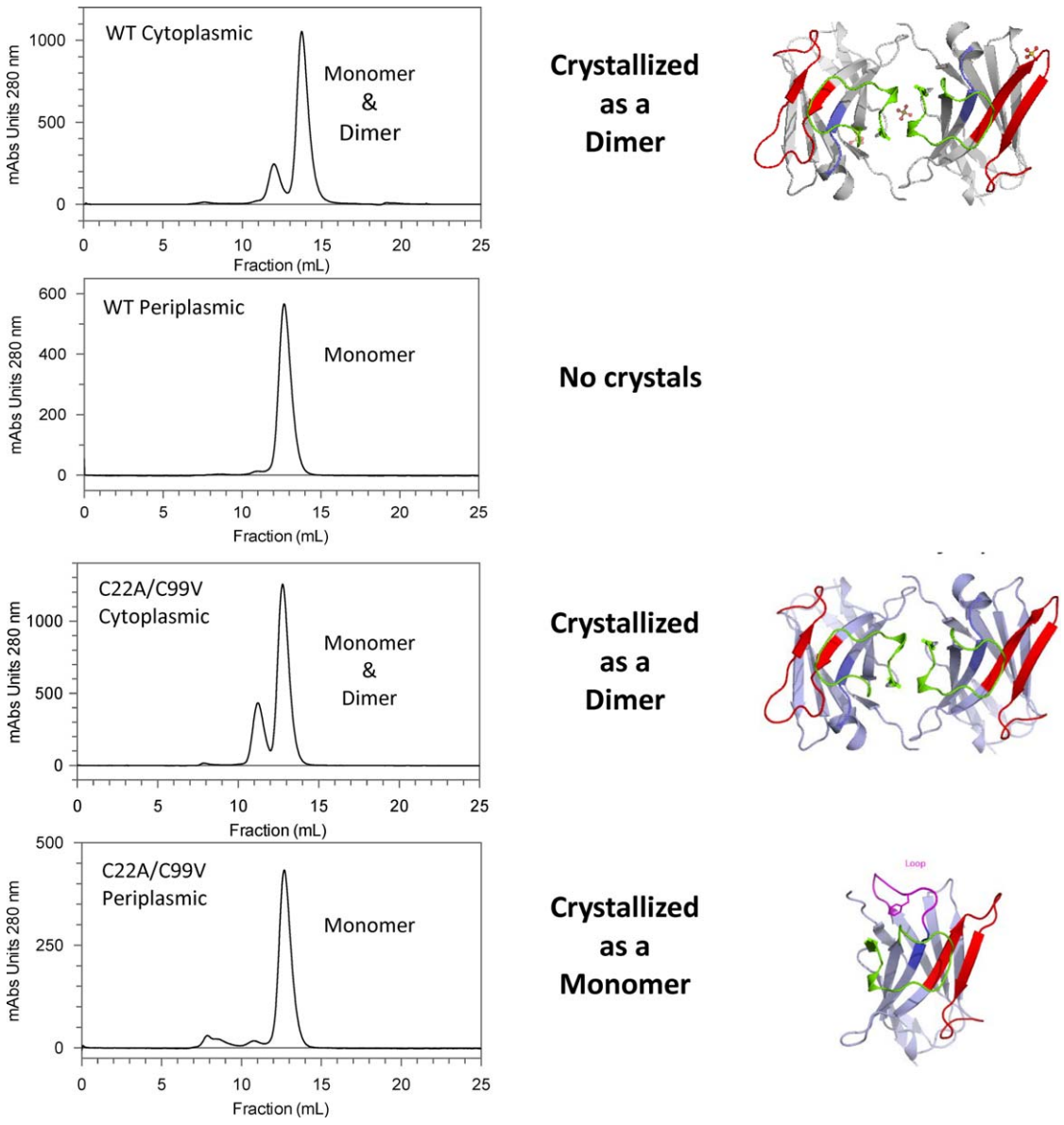

Figure 1

Effect of periplasmic vs. cytoplasmic expression on the quaternary structure of the thermostable WT sdAb A3 and its C22A/C99V variant. Protein expressed in the cytoplasm contained fractional amounts of homodimer, while protein produced in the periplasm was predominantly monomeric. The proteins containing dimer crystallized as asymmetric dimers, and the protein containing mostly monomer crystallized as a monomer. The CDR1 (R31-G35) is colored in blue, the CDR2 (A50-G69) is colored in red, and the CDR3 (D102-Y118) is colored in green. The backbone of the sdAb is colored in white for the WT protein and in slate blue for the C22A/C99V variant. The loop in magenta corresponds to a region where a difference in secondary structure was observed. The short helical region in the dimer was found as a loop in the structure of the monomer. The CDR2 loops of the dimer were found in two different conformations. The heart-shaped CDR2 loop is shown in the subunit on the left (A-form), and the β-hairpin CDR2 loop is shown in the subunit on the right (B-form). A sulfate ion was found in between the subunits of the WT dimer, but was not present in between the subunits of C22A/C99V disulfide-free variant. Figures were made using Pymol (Schrödinger, LLC).

(chain B, referred to as the B-form) (Fig. 2). The A and B forms did not show significant differences in side chain or backbone conformations outside of the CDR2 (root mean square deviation (r.m.s.d.) = 0.42 Å over 121 Cα out of 130). The B-factors for the asymmetric regions of the CDR2 loops were comparable to those of the hydrophobic core (Fig. 3, Supporting Information Fig. S2). The relatively low B-factors observed for these regions were not consistent with static or dynamic disorder; the CDR2 loops contained well-defined density.

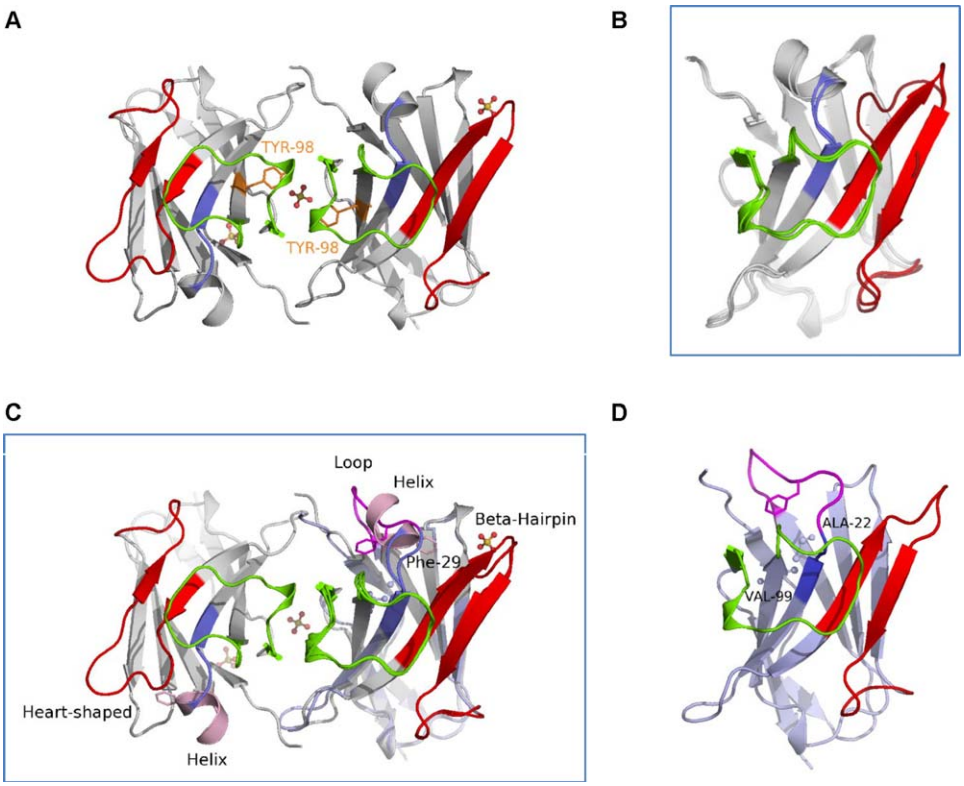

Figure 2

Structure of (**A**) the asymmetric WT homodimer (cytoplasmically produced) showing a large asymmetry in the CDR2 loops. Tyr-98 is shown in stick (orange). **B**: The overlay of the two subunits of the dimer (A-form and B-form) is shown in the box. The CDR2 loops (colored in red) differ in conformation. **C**: Overlay of the WT homodimer with the C22A/C99V monomer is shown in the box. Residues 24−33 can be found as a helix (pink) or a loop (magenta) in the dimer and the monomer, respectively. These residues carry a hydrophobic phenylalanine (F29, shown in stick). Phe-29 is found in two different local environments. **D**: The monomeric structure of the C22A/C99V variant (periplasmically produced protein). The region (residues 24−33) adjacent to the disulfide bond was found as a loop in the disulfide-bond free C22A/C99V variant. The location of the mutated Cys residues, Ala-22 and Val-99, are shown in gray ball and stick.

Disulfide bond status

Based upon distances and density, the disulfide bond in each WT monomer is broken in PDB 4TYU (Fig. 3). We also confirmed this in solution. Thiol titrations using Ellman's reagent[38] showed that the cytoplasmic protein utilized for crystallization contained partially reduced disulfide bonds, whereas the protein from the periplasm contained a fully formed disulfide (Fig. 3, Supporting Information Table S1). Two datasets were collected; one using a crystal which had been grown for 22 days (PDB 4TYU) and a second with a larger crystal grown over a 5-month period (PDB 4U7S) in the pH 4.1 crystallization condition. Omit maps were calculated using alanine in place of the cysteine residues (Fig. 3). The C22 and C99 residues could be refined separated without positive or negative difference density in the Fo-Fc map (3σ level). The Sγ atoms were spaced 3.56 and 3.48 Å apart in the A and B-forms, a distance significantly greater than a typical disulfide bond distance (2.03 Å[39]).

The A and B conformations of the protein were present in crystals containing partially reduced disulfides or the C22A/C99V mutations (no disulfide) (Fig. 1). A structure of a variant, S74A, showed slightly more disulfide bond density than in the WT A3 maps, but still carried asymmetric CDR2 loops [Fig. 3(C)]. The dimeric structure of the C22A/C99V variant purified from the cytoplasm confirmed that the asymmetry did not require a partially-formed disulfide bond.

WT protein purified from the periplasm contained a fully formed disulfide bond, and the protein was predominantly monomeric [Figs. 1 and 3(D)]. The C22A/C99V variant purified from the periplasm also was predominantly monomeric. For the cases shown in Figure 1, the quaternary structure depended on the type of expression and did not require a disulfide bond.

Monomeric structure of C22A/C99V

The heart-shaped loop of the A-form was not present in the monomeric structure. The structure of the monomeric C22A/C99V from the periplasm [Fig. 2(D)] contained a CDR2 loop with a β-hairpin and a

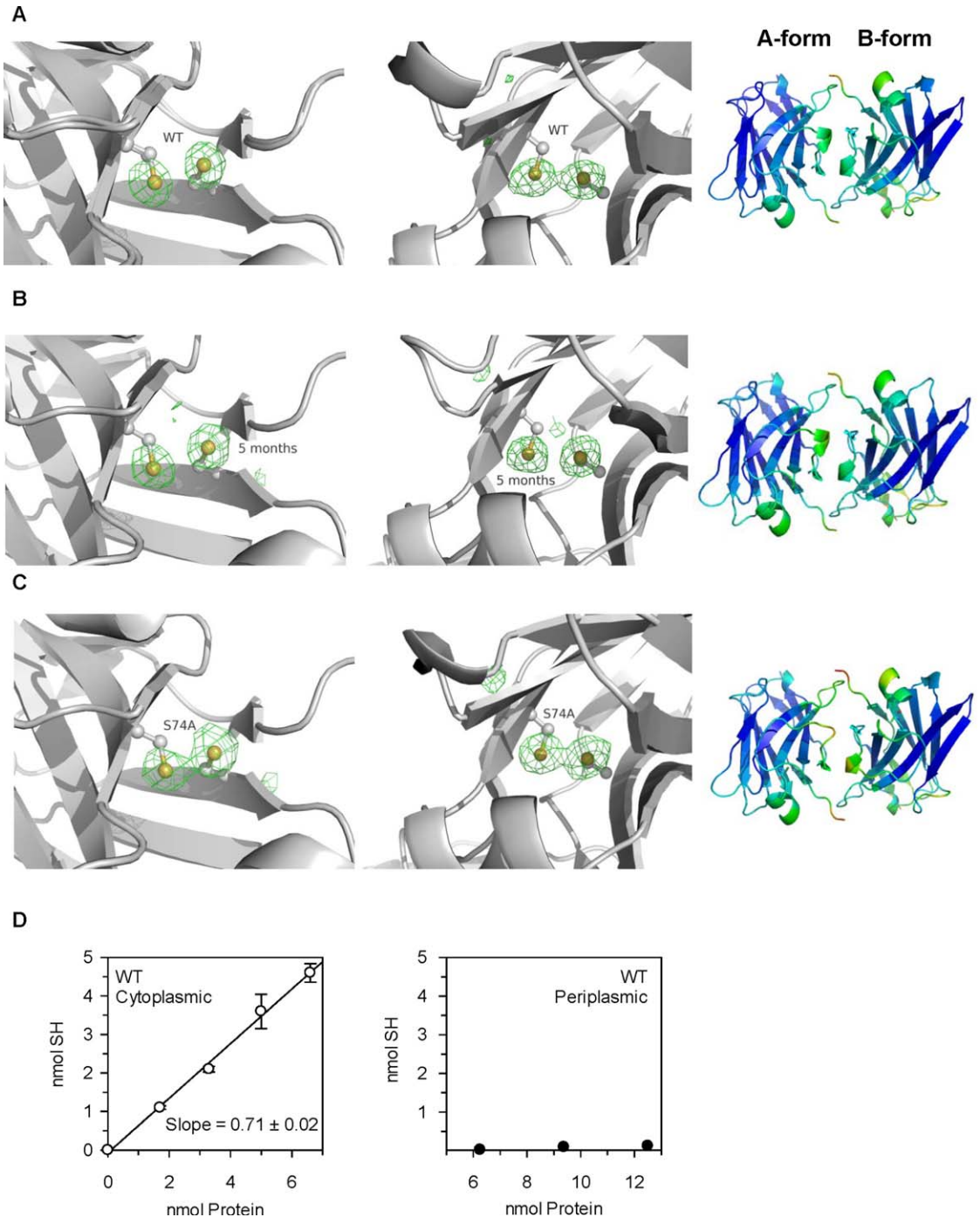

Figure 3

Omit maps (Fo-Fc difference density at the 3σ level) for the sulfurs of the disulfide bond (Cys-22:Cys-99) were calculated by substituting Ala in place of the Cys residues. Cysteines were then modeled into the density. The disulfide bond is progressively lost in the low pH crystallization condition; however, the conformational asymmetry between the A and B chains remains. The asymmetry was observed when the disulfide was partially reduced or completely absent (C22A/C99V). On the left are the disulfides of the A conformer, and on the right is the B conformer. **A**: Difference maps for the WT protein after 22 days of crystallization, and (**B**) after 5 months. **C**: In the S74A crystal more density for the disulfide is present, as is the conformational asymmetry. The structural asymmetry was also observed in the dimeric structure of the cytoplasmically expressed C22A/C99V variant, but not in the periplasmically expressed C22A/C99V variant (monomeric). **D**: In solution, the free thiols were titrated for the proteins expressed in the cytoplasm and periplasm. The disulfide was partially reduced in the cytoplasmically expressed protein (left) and fully formed in the periplasmically expressed protein (right).

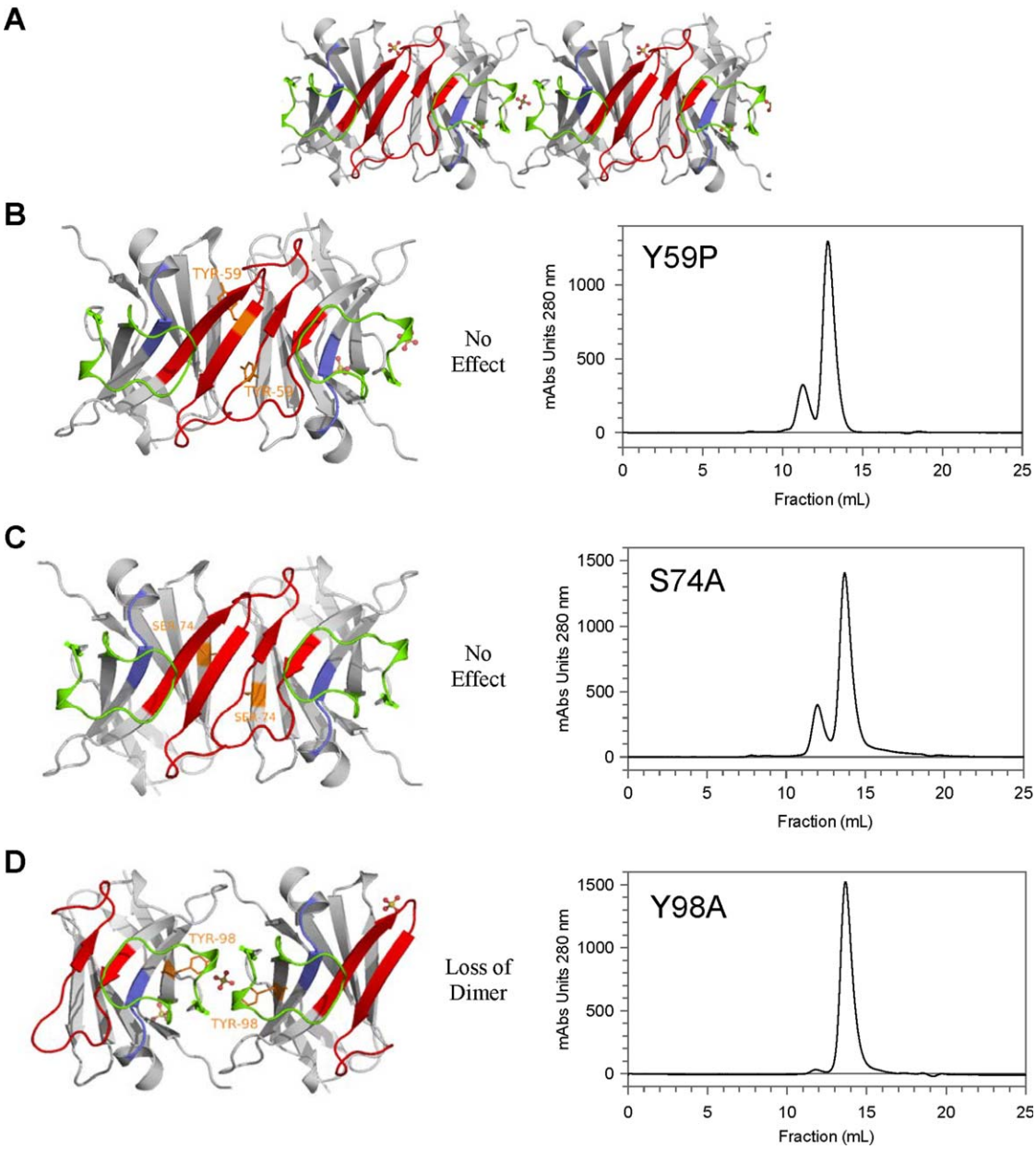

Figure 4

Determination of the predominant dimeric assembly(ies) present in solution using site-directed mutagenesis and a calibrated gel filtration column (G-75 Superdex). **A**: Packing in the crystal yielded two potential dimeric assemblies; the first assembly is shown in (**B**) and (**C**), and the second assembly is shown in (**D**). Chromatograms are shown on the right. In solution the (B) Y59P and (C) S74A mutations did not disrupt the dimer produced in the cytoplasm. D: The Y98A mutation produced mostly monomeric protein in the cytoplasm.

conformational difference in residues 24−33 which are located near the former site of the disulfide (r.m.s.d. = 0.61 Å over 116 Cα out of 130 Cα). Residues 24–33 were present at a crystal packing interface. The helical structure of residues 24−33 was not present in the monomeric C22A/C99V structure, but was present in the dimeric C22A/C99V structure suggesting a structurally dynamic region.

Determination of the quaternary structure in solution

The A and B forms alternate in the crystal. From the unusual packing in the crystal, two dimeric assemblies were predicted by PISA [Fig. 4(B) vs. 4(D)].[40,41] Crystals may have formed from multimers containing both species (e.g., 1-dimer and 1-monomer, etc.). Odd and even numbered multimers were observed in the Western blot using

high concentrations (16 mg/mL) of His-tagged sdAb A3 produced in the cytoplasm (Supporting Information Fig. S3). Contact areas of >600−850 Å^2 are typically found in biomolecular assemblies; however, the prediction of multimeric assemblies is more accurate when buried surface areas are larger than 6500 Å^2.[40] Contact surface areas were calculated by AreaImol with a probe radius of 1.4 Å.[42] The total contact surface area in the assembly shown in Figure 4(B) was ~3,541Å^2. The total contact surface area in the assembly shown in Figure 4(D) was ~3,566 Å^2. In the dimeric interface of Figure 4(D), 10 residues were within hydrogen bonding distance (≤3.8 Å), and one salt bridge was predicted (K43 and E1). In the dimeric interface of Figure 4(B), 12 residues were within hydrogen bonding distance, and no salt bridges were found. Since the contact areas were relatively small and comparable in both assemblies, the dimeric assembly(ies) present in solution at pH 7.4 was examined by gel filtration using a calibrated column and site-directed mutagenesis. Three variants, Y59P, S74A, and Y98A, were constructed. The mutations were selected based upon the crystal structure.

Proteins were purified without size-exclusion chromatography to >95% purity. The AKTA Purifier (G.E. Healthcare) system used here contains a 0.1 μm (100 nm) prefilter which prevents large aggregates from entering the column; the dimer is approximately 5.4−5.6 nm long across its longest dimension. Two peaks eluted from the calibrated gel filtration column when protein purified from the cytoplasm was loaded (Fig. 1); similar ratios of dimer to monomer have been reported previously for three other sdAb.[21–23] No buffer dependence was observed, as the dimer was observed in both 1x PBS pH 7.4 and 50 m*M* Tris pH 7.6, 150 m*M* NaCl. The monomer eluted at a volume corresponding to 14.1 kDa (calculated MW = 14.374 kDa), and the dimer eluted at a volume corresponding to 29.5 kDa (calculated MW = 28.748 kDa) in 1x PBS pH 7.4. SDS-PAGE gels (Supporting Information Fig. S3A) and tryptic peptide sequencing by tandem mass spectrometry (MS/MS) (Supporting Information Fig. S7) confirmed that the predominant protein present in both the monomer and dimer peaks eluting from the column was sdAb A3. No protein or metal impurities were found in SDS-PAGE gels (Supporting Information Fig. S3) or the electron density maps, respectively, consistent with non-covalent homodimer formation. A sulfate ion was found in the WT A3 dimer interface (Fig. 1), but was absent in the C22A/C99V dimer structure.

In the assembly of Figure 4(B), the β-strands of the framework regions of the A and B forms are within hydrogen bonding distance (S74 of the A-form and S72 of the B-form are 2.8−3.6 Å apart). The S74A dimer disruption mutation was predicted by the Robetta Server.[43] Ser-74 was mutated to alanine to remove the hydrogen bonding interaction. On the other face of the β-sandwich, the backbone NH and C═O groups of residues 58−63 of the CDR2 (colored red) of the B form and residues 58−61 of the CDR2 of the A form are within hydrogen bonding distance (7 potential hydrogen bonds total). A second mutation, Y59P, was selected to disrupt the β-sheet like structure formed at this interface. The dimeric species persisted for both of these variants suggesting that the assembly in Figure 4(B) was not the predominant dimer in solution.

In the assembly of Figure 4(D), the interface involves the CDR3 loops. CDR3 (D102-W119) consists of 17 residues and is of comparable length to other camelid CDR3. CDR3 loops have an average length of 15−17, 12, and 9 residues in camelid V_HH, human V_H, and mouse V_H, respectively.[3] The CDR3 of sdAb A3 forms an omega-shaped loop. Residues Q113−Y118 form a hinge which enables the loop to fold over the β-sheet; it covers 3 of the 4 β-strands including the variable residues of CDR1 and CDR2 [Fig. 2(B)]. The hinge region forms part of the dimeric interface and also involves conserved residues of the framework region: Y98, and E44 and R45 of the "V_HH tetrad." In an immunoglobulin the V_H and V_L dimerize and form a β-barrel. The V_HH tetrad refers to four residues within the framework which differ between human V_H and camelid V_HH at the former V_H/V_L interfacial surface. E44 and R45 are found in the more soluble camelid V_HH, while the less hydrophilic residues, G44 and L45, are found in human V_H. Typically, W47 of human V_H is replaced by less hydrophobic residues, and V37 of the core is replaced by a more hydrophobic F or Y residue. Camelization is the process of mutating the human V_H tetrad residues to those more commonly found in V_HH to improve solubility; in sdAb A3, E44 and R45 are part of the dimer interface, and R45 forms cation-pi interactions with Y98 and W119 at the interface.[44] The Y98A variant was monomeric, and no significant homodimer was observed using a protein concentration of 139 μ*M*. The Y98A mutation effectively led to the loss of the dimer, indicating that Tyr-98 plays a significant role in the stabilization of the dimer in solution.

While the CDR3 loop conformation could be found in several other V_HH structures by Dali,[45] the homodimeric assembly is not suggesting that residues outside of the CDR3 also are important for dimerization. One significant difference between a structurally similar sdAb, PDB 3STB,[46] and sdAb A3 occurred in the hinge, ^{111}SDE^{113}, and ^{113}QRS^{115}, respectively. In sdAb A3, R114 is near D117 of the opposing monomer. In 3STB the substitution of negatively charged residues in the hinge could create electrostatic repulsion and prevent homodimerization.

It was unclear why only a fraction of the protein (~10−20%) was able to form a dimer in solution. In attempts to measure an "apparent" K_d of the homodimer by size-exclusion chromatography, the concentration of loaded protein was varied (Fig. 5), and the area under the peaks was integrated to monitor the relative

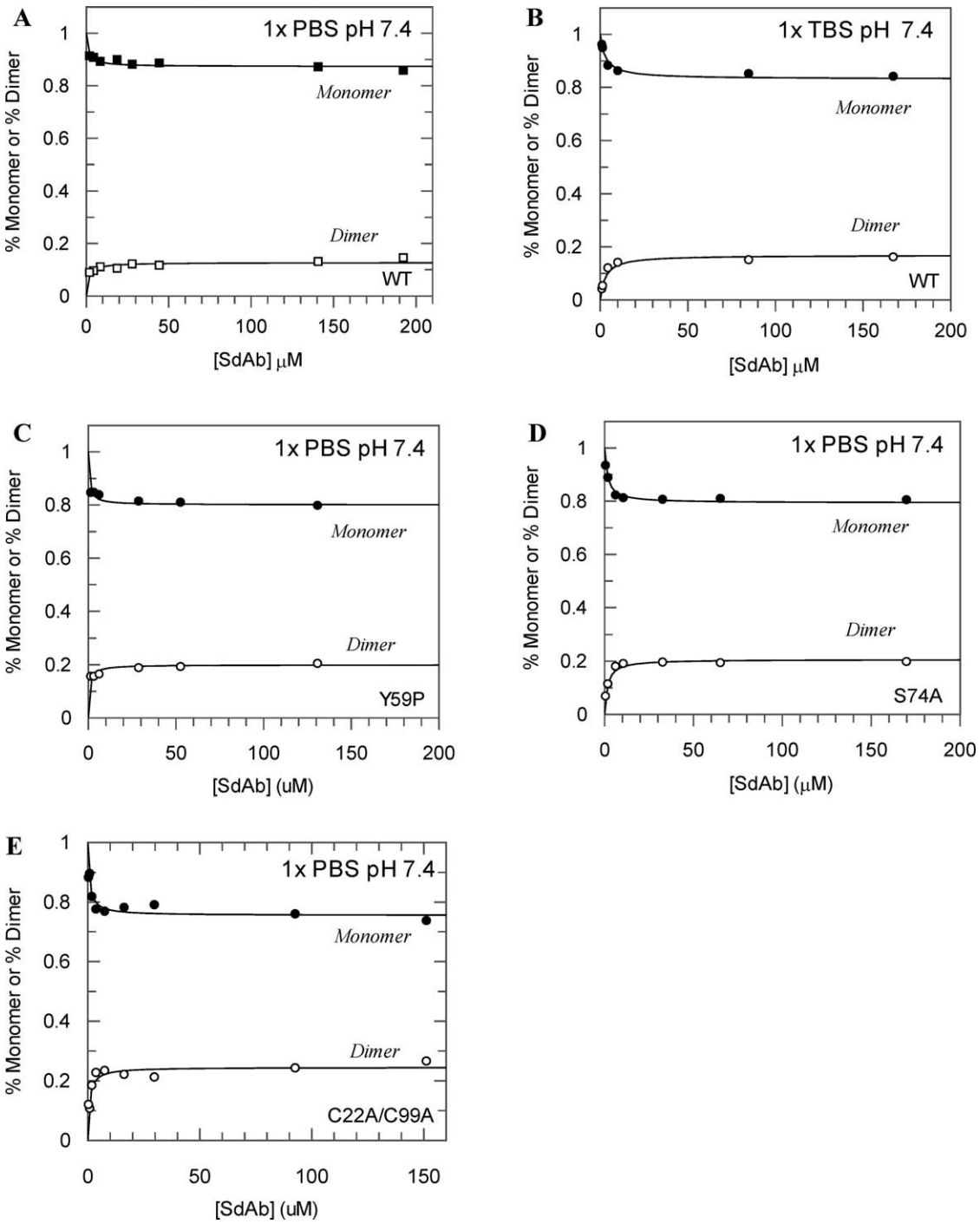

Figure 5

The concentrations of protein loaded onto the gel-filtration column were varied (*x*-axis), and the percentage of dimer and monomer were calculated from the peak areas. No increase in the percentage of dimer was observed at protein concentrations >50 μ*M*, and the concentration of dimer reached a plateau indicative of saturation. **A**: WT sdAb A3 cytoplasmically expressed was purified on a G-75 Superdex column equilibrated with 1x PBS pH 7.4, or (**B**) 1x TBS pH 7.4. No buffer dependence was observed. Variants of sdAb A3 were cytoplasmically expressed and purified with the same column equilibrated with 1x PBS 7.4. The (**C**) Y59P, (**D**) S74A, and (**E**) C22A/C99V are shown.

percentages of dimer and monomer. However, the separated monomer did not form additional dimer when reloaded onto the column (Supporting Information Fig. S7). Varying concentrations of the dimer did not lead to a significant concentration of monomer as the protein concentration was lowered, suggesting that dimer

Table II
Comparison of Melting Temperatures of WT A3 Constructs and Its Variants in 1x PBS pH 7.4

Protein	T_m (°C)	Expression	His-Tag	Quarternary Structure
WT	84.7 ± 0.1	Periplasm	–[a]	Monomer
WT	85.1 ± 0.1	Periplasm	C-terminal	Monomer
C22A/C99V	60 ± 1[b]	Periplasm	C-terminal	Monomer
WT	61.5 ± 0.3, 85.9 ± 0.4	Cytoplasm	NT-removed[c]	Dimer and Monomer
WT	61.8 ± 0.2, 87 ± 1	Cytoplasm	NT-removed	Purified Monomer
WT	58.9 ± 0.8, 82.1 ± 0.4	Cytoplasm	NT-removed	Purified Dimer
C22A/C99V	60.4 ± 0.7, 88 ± 4[b]	Cytoplasm	NT-removed	Dimer and Monomer
Y59P	62.8 ± 0.2, 91 ± 1	Cytoplasm	NT-removed	Dimer and Monomer
S74A	58.4 ± 0.3, 84.0 ± 0.6	Cytoplasm	NT-removed	Dimer and Monomer
Y98A	49.4 ± 0.3, 74.1 ± 0.3	Cytoplasm	NT-removed	Monomer

[a]No his-tag present in the protein sequence.
[b]Evidence of a second transition was present, but incomplete for accurate curve fitting.
[c]"NT-removed" indicates that the N-terminal His-tag was removed by thrombin cleavage.

dissociation was linked to irreversible processes such as aggregation or unfolding, or both. Thus, a true thermodynamic parameter could not be measured, as only the relative percentages of the soluble bound and free states could monitored. If the subunits of a dimer were weakly bound, the appearance of both dimer and monomer would suggest that the protein concentration was at or below the K_d of the dimer. When the percentages of monomer and dimer were measured, no increase in the percentage of dimer was observed as the protein concentration was raised above 50 μ*M*. Instead, a plateau was observed (Fig. 5). Changes in the percent dimer were observed below 2.4 μ*M* (Supporting Information Table S2). The plateau suggested saturation and tight binding. The fractional amount of homodimer indicated that a portion of the protein was conformationally distinct. The only observed conformational heterogeneities were in the CDR2 loop and residues 24−33 which were found as either a loop or helix in the C22A/C99V variant.

Melting temperatures of WT A3 constructs and its variants

SdAb A3 exhibited an unusually high T_m, approximately 20−25° higher than the average T_m of an sdAb. Using CD and differential scanning calorimetry (DSC) to monitor unfolding, two transitions ($T_{m1}^{app} = 61.5 \pm 0.3$ and $T_{m2}^{app} = 85.9 \pm 0.4$°C) were observed for the WT protein produced in the cytoplasm (Supporting Information Fig. S4, S5, Table II, Fig. 6). Evidence of two transitions was also observed with the cytoplasmic C22A/C99V protein, but the melting temperatures were less well resolved than in the WT and unfolding was less cooperative in the absence of the disulfide bond (Fig. 6). In contrast, periplasmic WT protein had a single transition ($T_m^{app} = 85.1 \pm 0.1$°C) and reversibly refolded (72% refolded after one cycle of heat denaturation). Reversibility depended strongly upon the disulfide bond. Thermal denaturation of the C22A/C99V variant produced in the cytoplasm or periplasm was irreversible, as was denaturation of the WT protein produced in the cytoplasm. Irreversible denaturation is characteristic of kinetically stable proteins,[13] but can also be observed for proteins possessing thermodynamic stability.

The two transitions were not unique to the dimer or monomer (Supporting Information Fig. S4). Both transitions were observed with the purified WT monomer and dimer as well as the Y98A variant (the cytoplasmically produced variant which was predominantly monomeric) (Table II).

The two transitions may be linked to the two different conformations (nonhelical and helical) of residues A24-A33 adjacent to the disulfide bond (C22/C99) (Fig. 2). The loop carries a hydrophobic residue, Phe-29, which is exposed in the monomer and buried in the dimer. Comparison of the periplasmically produced WT and C22A/C99V variant (both of which were predominantly monophasic) suggested that the loss of the disulfide may lead to a 25°C decrease in the T_m^{app} (Fig. 6). This decrease may be due to both the loss of the disulfide bond and loss of this helix. Other sdAb mutated to prevent the formation of the conserved disulfide have had similar reductions in their T_m ~10−20°C.[47,48]

Y98A was the most poorly produced A3 variant of the ones tested. However, the soluble protein obtained was monomeric and could be concentrated to 139 μ*M* without evidence of significant aggregation in the chromatogram [Fig. 4(D)]. Y98A had a 12°C decrease in the T_m, which may be due to the loss of a cation-pi interaction[44] with R45 of the tetrad. In one of our low T_m structures of an anti-cholera toxin sdAb (PDB 4IDL, $T_m = 46$°C),[49] the R45 and Y98 residues could be found in a similar orientation within a monomeric protein. Thus, the intramolecular interaction of these residues is not specific to A3. The monomeric nature of the Y98A variant suggests that the Tyr-98 residue plays an important role in intermolecular interactions which stabilize the dimer.

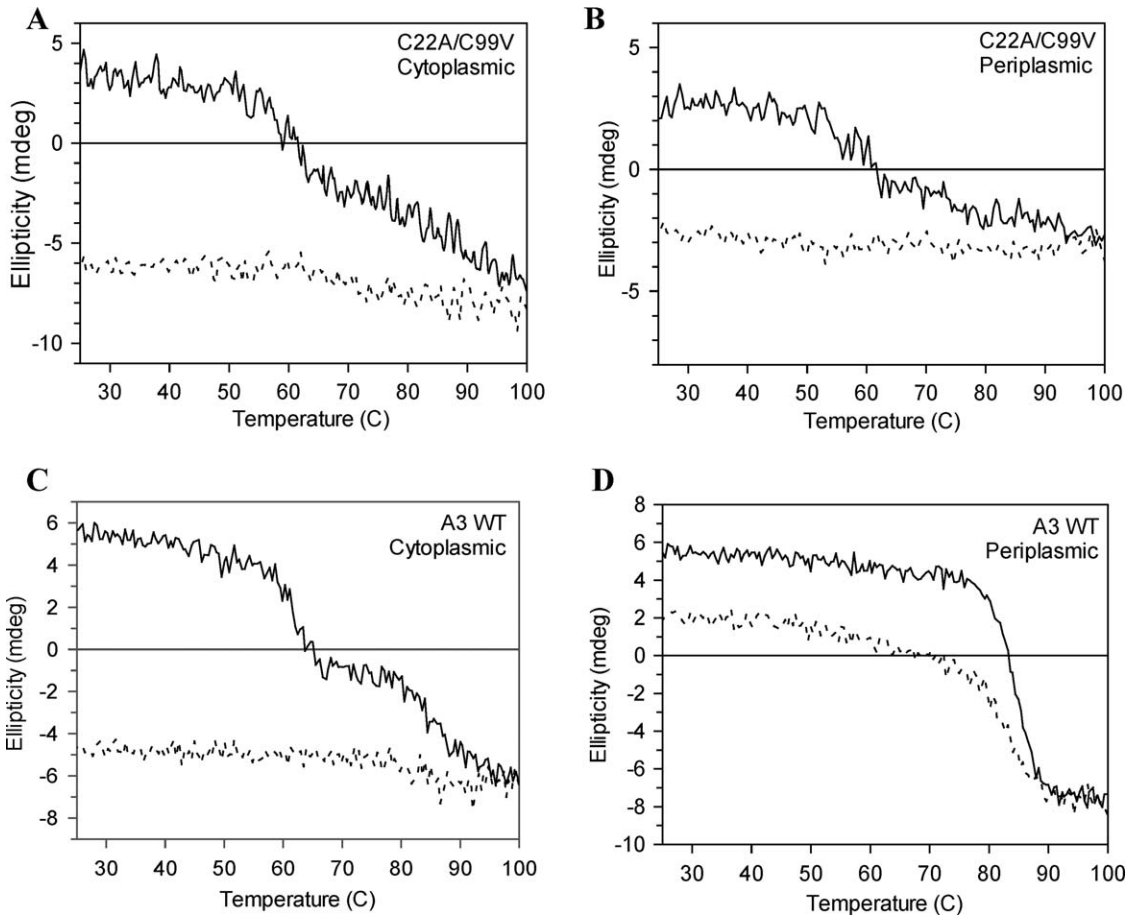

Figure 6

Thermal denaturation of A3 monitored by CD spectroscopy. Two transitions are observed for the protein produced in the cytoplasm, while only the high temperature transition is observed with the protein produced in the periplasm. (**A**) and (**B**) are melting curves for the C22A/C99V variant expressed in the cytoplasm and periplasm, respectively. The heating (black line) and cooling (dots) are shown. Unfolding was irreversible in the absence of a fully formed disulfide bond. In the absence of the disulfide bond (C22A/C99V), a similar break between two transitions was observed in (A), and unfolding was less cooperative. **C**: WT sdAb A3 expressed in the cytoplasm (the N-terminal his-tag was removed) irreversibly unfolded, and two transitions were observed. **D**: Only WT sdAb A3 expressed in the periplasm refolded reversibly with a single transition. Protein from the periplasm contained a fully formed disulfide. Reversible refolding depended strongly on the disulfide. The two transitions may be due to a region between residues 24−33 which was helical in the dimer and nonhelical in the monomeric structure of the disulfide-bond free C22A/C99V variant.

DISCUSSION

Within the literature there are 3 reports of partial dimerization of v-set domains.[21–23] Here we have shown that the percentage of the dimeric fraction does not increase as the protein is concentrated, indicating that the species able to form the dimer is saturated and tightly bound (Fig. 5). No evidence of coordinated metals or other small molecule contaminants were found in the electron density. The dimeric fraction did not depend upon the buffer used in gel-filtration, and the dimer and monomer were found to be comparably pure by SDS-PAGE (Supporting Information Fig. S3A). The observed partial homodimerization indicated the presence of a conformationally distinct species. We hypothesized that the conformational heterogeneity may be linked to the partial reduction of the disulfide and protein misfolding in the cytoplasm and tested this hypothesis by expressing the WT and C22A/C99V proteins in the periplasm and cytoplasm. We found that the formation of the dimer was dependent upon the method of expression and that the dimer could form when the disulfide was partially reduced or completely absent (Fig. 1).

In the structure of the C22A/C99V monomer, the A-form of the CDR2 loop was not observed autonomously. Instead, a β-hairpin similar to that of the B-form was observed (Fig. 2). Structural similarity to the heart-shaped loop was not found in Dali searches[45]; in contrast, CDR2 structures with β-hairpins were more

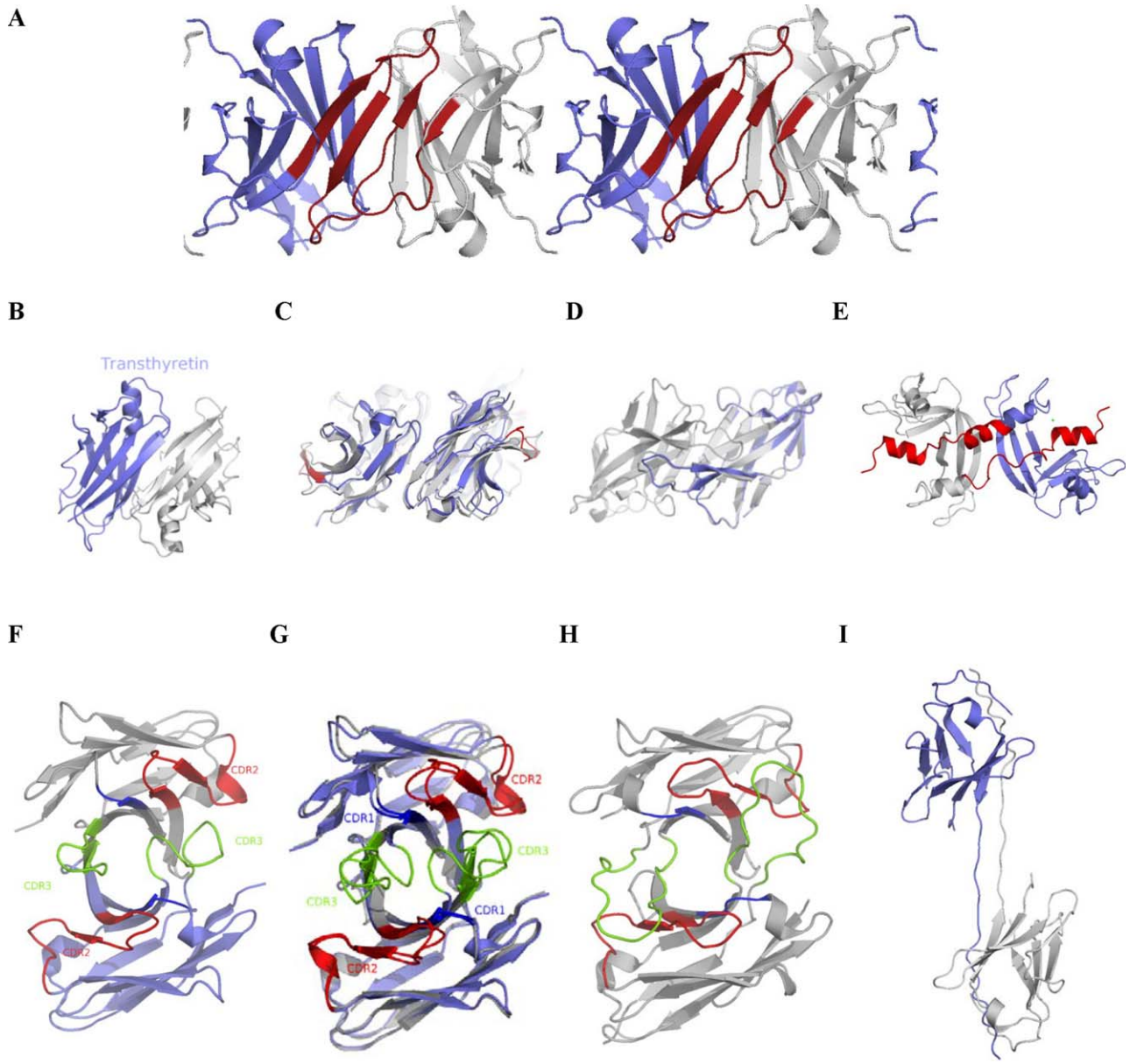

Figure 7

Structural comparisons. **A**: Packing of the pleomorphic forms of V_HH A3 in the crystal. **B**: The amyloidogenic protein transthyretin elutes as mixtures of soluble monomer, dimer, and higher multimers.[50,64] **C**: The structure of VH-B1a (PDB 3B9V).[21] Overlay of the domains shows one region (red) containing a difference in secondary structure. **D**: Domain swapped dimer of a shark V_{NAR} (PDB 1VES).[23] Overlay of the two molecules of the ASU showed minor differences in the backbone. **E**: Two molecules of the asymmetric unit of bovine pancreatic ribonuclease A (PDB 1A2W) show the loss of a helical segment in one subunit. Staining of these crystals with Congo Red has been reported,[65] and the protein eluted as a mixture of monomer and dimer from a HPLC size exclusion column.[65] **F**: Human V_H HEL4 (PDB 1OHQ)[22] is mostly monomeric in solution, but crystallizes with two molecules per ASU in a β-barrel. Its mutants, S35G and W47R, contain higher amounts (10−15%) of dimer. **G**: Overlay of the two molecules in the ASU shows an asymmetry in the CDR3 loops, but a β-barrel structure similar to that of a typical V_H/V_L β-barrel. **H**: Homodimeric structure of Gr6.[24] The packing is similar to that of a V_H/V_L β-barrel. Gr6 elutes as a dimer only. **I**: Homodimeric structure of V_HH (PDB 1SJV) showing a third type of domain-swapped dimer.[29] Proteins in (A), (B), (C), (D), and (E) showed fractional amounts of dimer in gel-filtration column chromatograms. Mutants of (F) produced fractional amounts of dimer. Protein in (H) was completely homodimeric.

populated states within the PDB. The A-form or the A-B dimer may represent a metastable misfolded state. The fibril-like packing of the dimer in the crystal and the laddering in SDS-PAGE gels also was unusual. Two of the β-strands of the framework regions were oriented nearly perpendicular to the axis of the linear protein assemblies in the lattice (Supporting Information Fig. S3). This is notable since cross-β and β-helical structures contain β-strands oriented perpendicular or nearly perpendicular to the axis of the fibril. This structural feature has been

proposed to be common to proteins associated with misfolding diseases.[50–52]

One feature that was common to 3 of the sdAb proteins, which were able to form fractional amounts of dimer and had reported structures, was that their dimeric structures differed from the typical β-barrel of V_H/V_L heterodimers [Fig. 7(A,C,D)]. HEL4, which was mostly monomeric in solution, crystallized as a β-barrel [Fig. 7(F,G)]. Gr6, on the other hand, was predominantly dimeric and crystallized as a β-barrel [Fig. 7(H)]. The packing of the three proteins which formed fractional amounts of dimers was reminiscent of transthyretin, a well-known example of a protein prone to misfolding[50] [Fig. 7(B)].

Subtly misfolded aberrant conformations have been thought to be associated with rare protein misfolding diseases[10,53,54] (Reviewed in Ref. [55]). Crystal contacts can affect loop conformations. From a static crystal structure, we cannot determine if the crystal formed because the conformer(s) had a higher propensity to pack, or if the packing distorted the loop conformation(s). However, in this case, regardless of the crystallization experiments, the conformationally distinct species able to form the dimer was observed in solution eluting from the gel-filtration column. V-set domains are known to misfold; for example, the human heavy and light chains cause heavy[26] and light chain amyloidosis.[25,28] Unpaired heavy (V_H) and light chains (V_L, also known as Bence-Jones proteins)[56] are not normally produced *in vivo*; they have only been found to be overexpressed in very rare proliferative B-cell disorders such as multiple myeloma.[26,57] The atypical unpaired monoclonal light chains can form amyloid in the kidneys if continuously produced at high concentrations by cancerous cells.[28,57] The high concentrations of light chain in the serum combined with the low pH of urine (typically pH 4.5−5.0 after the removal of bicarbonate) favors amyloid fibril formation there.[58] Amyloid-like fibril formation has been associated with the reduction of the disulfide.[59]

Heterologous expression of mammalian proteins in bacteria is not always successful. Undesireable protein−protein interactions can impact the production, handling, storage, and evaluation of antibodies used in immunoasssays or as biopharmaceuticals.[60] Here we have shown that bacterial cytoplasmic expression can lead to a stable dimeric state with a partially reduced disulfide or a mutated disulfide (C22A/C99V). More importantly, we demonstrate that the dimeric species can be avoided by periplasmic expression and full disulfide bond formation. This finding may argue against low pH elution (pH 3.0) and cytoplasmic expression of these domains, both of which can compromise the disulfide bond. We hypothesize that the asymmetric dimeric structure may represent a kinetically stable misfolded state. The behavior of the sdAb A3 protein in solution and in the crystalline state may yield new insight into existing models[51,61–63] and mechanisms of multimerization which involve distortions of the β-strands on the edges of β-sheets.

ACKNOWLEDGMENTS

The opinions expressed here are those of the authors and do not represent those of the U.S. Army, U.S. Navy, U.S. Department of Defense, or the U.S. government. We are grateful to Dr. Kendrick Turner for providing the C22A/C99V plasmids, and Drs. Ellen R. Goldman and George P. Anderson for helpful discussions and support of this project.

REFERENCES

1. Harpaz Y, Chothia C. Many of the immunoglobulin superfamily domains in cell adhesion molecules and surface receptors belong to a new structural set which is close to that containing variable domains. J Mol Biol 1994;238:528–539.
2. Eyer L, Hruska K. Single-domain antibody fragments derived from heavy-chain antibodies: a review. In: 2012. 513 p.
3. Dumoulin M, Conrath K, Van MA, Meersman F, Heremans K, Frenken LG, Muyldermans S, Wyns L, Matagne A. Single-domain antibody fragments with high conformational stability. Protein Sci 2002;11:500–515.
4. Perez JM, Renisio JG, Prompers JJ, van Platerink CJ, Cambillau C, Darbon H, Frenken LG. Thermal unfolding of a llama antibody fragment: a two-state reversible process. Biochemistry 2001;40:74–83.
5. Graef RR, Anderson GP, Doyle KA, Zabetakis D, Sutton FN, Liu JL, Serrano-Gonzalez J, Goldman ER, Cooper LA. Isolation of a highly thermal stable lama single domain antibody specific for Staphylococcus aureus enterotoxin B. BMC Biotechnol 2011;11:86.
6. Razvi A, Scholtz JM. Lessons in stability from thermophilic proteins. Protein Sci 2006;15:1569–1578.
7. Rees DC, Robertson AD. Some thermodynamic implications for the thermostability of proteins. Protein Sci 2001;10:1187–1194.
8. Baker D, Agard DA. Kinetics versus thermodynamics in protein folding. Biochemistry 1994;33:7505–7509.
9. Baker D, Sohl JL, Agard DA. A protein-folding reaction under kinetic control. Nature 1992;356:263–265.
10. Sanchez-Ruiz JM. Protein kinetic stability. Biophys Chem 2010;148:1–15.
11. Lumry R, Eyring H. Conformation Changes of Proteins. J Phys Chem 1954;58:110–120.
12. Milardi D, La RC, Grasso D. Extended theoretical analysis of irreversible protein thermal unfolding. Biophys Chem 1994;52:183–189.
13. Sanchez-Ruiz JM. Theoretical analysis of Lumry-Eyring models in differential scanning calorimetry. Biophys J 1992;61:921–935.
14. Baldwin AJ, Knowles TP, Tartaglia GG, Fitzpatrick AW, Devlin GL, Shammas SL, Waudby CA, Mossuto MF, Meehan S, Gras SL, Christodoulou J, Nthony-Cahill SJ, Barker PD, Vendruscolo M, Dobson CM. Metastability of native proteins and the phenomenon of amyloid formation. J Am Chem Soc 2011;133:14160–14163.
15. Cunningham EL, Jaswal SS, Sohl JL, Agard DA. Kinetic stability as a mechanism for protease longevity. Proc Natl Acad Sci USA 1999;96:11008–11014.
16. Jaswal SS, Sohl JL, Davis JH, Agard DA. Energetic landscape of alpha-lytic protease optimizes longevity through kinetic stability. Nature 2002;415:343–346.
17. Manning M, Colon W. Structural basis of protein kinetic stability: resistance to sodium dodecyl sulfate suggests a central role for

rigidity and a bias toward beta-sheet structure. Biochemistry 2004; 43:11248–11254.
18. Plaza dP, I, Ibarra-Molero B, Sanchez-Ruiz JM. Lower kinetic limit to protein thermal stability: a proposal regarding protein stability in vivo and its relation with misfolding diseases. Proteins 2000;40:58–70.
19. Rho H, Jones CN, Rose RB. Kinetic stability may determine the interaction dynamics of the bifunctional protein DCoH1, the dimerization cofactor of the transcription factor HNF-1alpha. Biochemistry 2010;49:10187–10197.
20. Turner KB, Zabetakis D, Goldman ER, Anderson GP. Enhanced stabilization of a stable single domain antibody for SEB toxin by random mutagenesis and stringent selection. Protein Eng Des Sel 2014; 27:89–95. doi: 10.1093/protein/gzu001. Epub 2014 Jan 30.
21. Barthelemy PA, Raab H, Appleton BA, Bond CJ, Wu P, Wiesmann C, Sidhu SS. Comprehensive analysis of the factors contributing to the stability and solubility of autonomous human VH domains. J Biol Chem 2008;283:3639–3654.
22. Jespers L, Schon O, James LC, Veprintsev D, Winter G. Crystal structure of HEL4, a soluble, refoldable human V(H) single domain with a germ-line scaffold. J Mol Biol 2004;337:893–903.
23. Streltsov VA, Varghese JN, Carmichael JA, Irving RA, Hudson PJ, Nuttall SD. Structural evidence for evolution of shark Ig new antigen receptor variable domain antibodies from a cell-surface receptor. Proc Natl Acad Sci USA 2004;101:12444–12449.
24. Baral TN, Chao SY, Li S, Tanha J, rbabi-Ghahroudi M, Zhang J, Wang S. Crystal structure of a human single domain antibody dimer formed through V(H)-V(H) non-covalent interactions. PLoS One 2012;7:e30149.
25. Cohen AD, Comenzo RL. Systemic light-chain amyloidosis: advances in diagnosis, prognosis, and therapy. Hematol Am Soc Hematol Educ Program 2010;2010:287–294.
26. Eulitz M, Weiss DT, Solomon A. Immunoglobulin heavy-chain-associated amyloidosis. Proc Natl Acad Sci USA 1990;87:6542–6546.
27. Isobe T, Kametani F, Shinoda T. V-domain deposition of lambda Bence Jones protein in the renal tubular epithelial cells in a patient with the adult Fanconi syndrome with myeloma. Amyloid 1998;5: 117–120.
28. Sanchorawala V. Light-chain (AL) amyloidosis: diagnosis and treatment. Clin J Am Soc Nephrol 2006;1:1331–1341.
29. Spinelli S, Desmyter A, Frenken L, Verrips T, Tegoni M, Cambillau C. Domain swapping of a llama VHH domain builds a crystal-wide beta-sheet structure. FEBS Lett 2004;564:35–40.
30. Kortemme T, Kim DE, Baker D. Computational alanine scanning of protein-protein interfaces. Sci STKE 2004;2004:l2.
31. McCoy AJ, Grosse-Kunstleve RW, Adams PD, Winn MD, Storoni LC, Read RJ. Phaser crystallographic software. J Appl Crystallogr 2007;40:658–674.
32. Arnold K, Bordoli L, Kopp J, Schwede T. The SWISS-MODEL workspace: a web-based environment for protein structure homology modelling. Bioinformatics 2006;22:195–201.
33. Kiefer F, Arnold K, Kunzli M, Bordoli L, Schwede T. The SWISS-MODEL Repository and associated resources. Nucleic Acids Res 2009;37:D387–D392.
34. Emsley P, Cowtan K. Coot: model-building tools for molecular graphics. Acta Crystallogr D Biol Crystallogr 2004;60:2126–2132.
35. Emsley P, Lohkamp B, Scott WG, Cowtan K. Features and development of Coot. Acta Crystallogr D Biol Crystallogr 2010;66: 486–501.
36. Brünger AT, Adams PD, Clore GM, DeLano WL, Gros P, Grosse-Kunstleve RW, Jiang JS, Kuszewski J, Nilges M, Pannu NS, Read RJ, Rice LM, Simonson T, Warren GL. Crystallography & NMR system: a new software suite for macromolecular structure determination. Acta Crystallogr D Biol Crystallogr 1998;54:905–921.
37. Collaborative Computational Project N4. The CCP4 suite: programs for protein crystallography. Acta Crystallogr D Biol Crystallogr 1994;50:760–763.
38. Legler PM, Leary DH, Hervey WJ, Millard CB. A role for His-160 in peroxide inhibition of S. cerevisiae S-formylglutathione hydrolase: evidence for an oxidation sensitive motif. Arch Biochem Biophys 2012;528:7–20.
39. Hazes B, Dijkstra BW. Model building of disulfide bonds in proteins with known three-dimensional structure. Protein Eng 1988;2:119–125.
40. Krissinel E. Crystal contacts as nature's docking solutions. J Comput Chem 2010;31:133–143.
41. Krissinel E, Henrick K. Inference of macromolecular assemblies from crystalline state. J Mol Biol 2007;372:774–797.
42. Lee B, Richards FM. The interpretation of protein structures: estimation of static accessibility. J Mol Biol 1971;55:379–400.
43. Kim DE, Chivian D, Baker D. Protein structure prediction and analysis using the Robetta server. Nucleic Acids Res 2004;32:W526–W531.
44. Gallivan JP, Dougherty DA. Cation-pi interactions in structural biology. Proc Natl Acad Sci USA 1999;96:9459–9464.
45. Holm L, Rosenstrom P. Dali server: conservation mapping in 3D. Nucleic Acids Res 2010;38:W545–W549.
46. Park YJ, Pardon E, Wu M, Steyaert J, Hol WG. Crystal structure of a heterodimer of editosome interaction proteins in complex with two copies of a cross-reacting nanobody. Nucleic Acids Res 2012;40: 1828–1840.
47. Hagihara Y, Mine S, Uegaki K. Stabilization of an immunoglobulin fold domain by an engineered disulfide bond at the buried hydrophobic region. J Biol Chem 2007;282:36489–36495.
48. Saerens D, Conrath K, Govaert J, Muyldermans S. Disulfide bond introduction for general stabilization of immunoglobulin heavy-chain variable domains. J Mol Biol 2008;377:478–488.
49. Legler PM, Zabetakis D, Anderson GP, Lam A, Hol WG, Goldman ER. Structure of a low-melting-temperature anti-cholera toxin: llama V(H)H domain. Acta Crystallogr Sect F Struct Biol Cryst Commun 2013;69:90–93.
50. Eneqvist T, Andersson K, Olofsson A, Lundgren E, Sauer-Eriksson AE. The beta-slip: a novel concept in transthyretin amyloidosis. Mol Cell 2000;6:1207–1218.
51. Jahn TR, Makin OS, Morris KL, Marshall KE, Tian P, Sikorski P, Serpell LC. The common architecture of cross-beta amyloid. J Mol Biol 2010;395:717–727.
52. Sunde M, Serpell LC, Bartlam M, Fraser PE, Pepys MB, Blake CC. Common core structure of amyloid fibrils by synchrotron X-ray diffraction. J Mol Biol 1997;273:729–739.
53. Dobson CM. Protein misfolding, evolution and disease. Trends Biochem Sci 1999;24:329–332.
54. Kelly JW. The alternative conformations of amyloidogenic proteins and their multi-step assembly pathways. Curr Opin Struct Biol 1998;8:101–106.
55. Bradbury J. Chaperones: keeping a close eye on protein folding. Lancet 2003;361:1194–1195.
56. Epp O, Colman P, Fehlhammer H, Bode W, Schiffer M, Huber R, Palm W. Crystal and molecular structure of a dimer composed of the variable portions of the Bence-Jones protein REI. Eur J Biochem 1974;45:513–524.
57. Sattianayagam P, Gibbs S, Hawkins P, Gillmore J. Systemic AL (light-chain) amyloidosis and the gastrointestinal tract. Scand J Gastroenterol 2009;44:1384–1385.
58. Dember LM. Amyloidosis-associated kidney disease. J Am Soc Nephrol 2006;17:3458–3471.
59. Klafki HW, Pick AI, Pardowitz I, Cole T, Awni LA, Barnikol HU, Mayer F, Kratzin HD, Hilschmann N. Reduction of disulfide bonds in an amyloidogenic Bence Jones protein leads to formation of "amyloid-like" fibrils in vitro. Biol Chem Hoppe Seyler 1993;374: 1117–1122.

60. Yearley EJ, Godfrin PD, Perevozchikova T, Zhang H, Falus P, Porcar L, Nagao M, Curtis JE, Gawande P, Taing R, Zarraga IE, Wagner NJ, Liu Y. Observation of small cluster formation in concentrated monoclonal antibody solutions and its implications to solution viscosity. Biophys J 106:1763–1770.
61. Laidman J, Forse GJ, Yeates TO. Conformational change and assembly through edge + strands in transthyretin and other amyloid proteins. Acc Chem Res 2006;39:576–583.
62. Larini L, Shea JE. Role of beta-hairpin formation in aggregation: the self-assembly of the amyloid-beta(25–35) peptide. Biophys J 2012;103:576–586.
63. Richardson JS, Richardson DC. Natural +sheet proteins use negative design to avoid edge-to-edge aggregation. Proceedings of the National Academy of Sciences 2002;99:2754–2759.
64. Olofsson A, Ippel JH, Wijmenga SS, Lundgren E, Ohman A. Probing solvent accessibility of transthyretin amyloid by solution NMR spectroscopy. J Biol Chem 2004;279:5699–5707.
65. Liu Y, Hart PJ, Schlunegger MP, Eisenberg D. The crystal structure of a 3D domain-swapped dimer of RNase A at a 2.1-A resolution. Proc Natl Acad Sci USA 1998;95:3437–3442.